Optical Probing of Rayleigh Wave Driven Magnetoacoustic Resonance

P. Kuszewski,[1] J.-Y. Duquesne,[1] L. Becerra,[1] A. Lemaître,[2] S. Vincent,[1] S. Majrab,[1] F. Margaillan,[1] C. Gourdon,[1] and L. Thevenard[1,*]

[1] *Sorbonne Université, CNRS, Institut des Nanosciences de Paris, 4 place Jussieu 75252 Paris, France*

[2] *Centre de Nanosciences et de Nanotechnologies, CNRS, Université Paris-Sud, Université Paris-Saclay, 91460 Marcoussis, France*

(Received 1 June 2018; published 19 September 2018)

The resonant interaction of electrically excited traveling surface acoustic waves and magnetization has hitherto been probed through the acoustic component. In this work we investigated it using time-resolved magneto-optical detection of magnetization dynamics. To that end, we develop an experimental scheme where laser pulses are used both to generate the acoustic wave frequency and to probe magnetization dynamics, thus ensuring perfect phase locking. The light-polarization dependence of the signal enables us to disentangle elasto-optical and magneto-optical contributions and to obtain the in-plane and out-of-plane components of the magnetization dynamics. Magnetization precession is proven to be driven solely by the acoustic wave. Its amplitude is shown to resonate at the same field at which we detect piezoelectrically the resonant attenuation of the acoustic wave, clearly evidencing the magnetoacoustic resonance with high sensitivity.

DOI: 10.1103/PhysRevApplied.10.034036

I. INTRODUCTION

Recent years have witnessed renewed and growing interest in the use of acoustic waves to excite spin waves as an alternative, fast, efficient, and heat-free means to generate and control (possibly coherently and remotely) information in magnetic materials [1–16]. Magnetization switching [3,7,11,12,16] and parametric excitation of spin waves [9,13] have, for instance, been demonstrated, thus opening new opportunities for applications. The efficiency of acoustic waves relies on magnetoelastic coupling that occurs in magnetostrictive materials. Electrically excited surface acoustic waves (SAWs), with typical frequencies up to the gigahertz range, are particularly well suited to excite magnetization dynamics in ferromagnetic magnetostrictive layers. Their interaction was evidenced by piezoelectric detection of SAW-induced ferromagnetic resonance (SAW-FMR) [1,4]: the SAW amplitude and velocity resonantly decrease when the spin-wave frequency is varied across the SAW frequency by an applied magnetic field. However, spin waves have not been concomitantly observed. Time-resolved detection of magneto-optical effects using probe laser pulses could provide a direct and very sensitive method to access magnetization dynamics [17]. This requires a nontrivial synchronization of the electrical SAW generation with probe laser pulses. Until now this difficulty has been bypassed by use of fairly cumbersome synchrotron x-ray radiation [18]. However, no resonant magnetization dynamics have been observed.

In this article, we demonstrate optically the forced magnetic precession induced by traveling SAWs. To that end, we implement a tabletop setup to generate SAW bursts electrically using interdigitated transducers (IDTs) with perfect phase locking to laser pulses, which enables the optical investigation of time- and space-resolved magnetization dynamics excited by the SAW. We illustrate the potentiality of this technique using a ferromagnetic semiconductor layer of (Ga,Mn)As on piezoelectric GaAs, taking advantage of its low FMR frequency, which is easily tunable across the SAW frequency, and its sizable magneto-optical effects. Using the probe-light polarization and the magnetic field dependencies of the time-resolved signal, we separate the magneto-optical contribution from the pure elasto-optical contribution. The in-plane and out-of plane components of the magnetization dynamics display the dependencies on the magnetic field expected from the SAW-induced torque acting on the magnetization [19,20]. Finally, we show that resonant magnetic excitation appears concomitantly with resonant SAW absorption, the detection of the former being more sensitive than that of the latter.

II. EXPERIMENTAL SETUP

SAWs such as Rayleigh waves are easy to implement and thus find applications in various fields of soft- and condensed-matter physics [21–24]. With frequencies up

*thevenard@insp.jussieu.fr

to the gigahertz range, their dynamical strain components are confined within a few microns from the surface, and can thus efficiently interact with a magnetic layer on a substrate. SAWs can be generated either optically via thermoelasticity [5,10,13,25] or electrically via the piezoelectric effect with the use of IDTs [26,27]. The simplest IDT consists of two comb-shaped electrodes in a zipper configuration that work as capacitors on a piezoelectric surface. When a radio-frequency (rf) voltage at f_{SAW} is applied, SAWs are generated and propagate on either side of the IDT. The wavelength λ_{SAW} of the excited rf is determined by the period of the electrode teeth. Frequency and wavelength are related by $\lambda_{\mathrm{SAW}} = v_R/f_{\mathrm{SAW}}$, where v_R is the Rayleigh velocity. Typical λ_{SAW} values are around a few microns. The strain components excited with the IDT are the longitudinal strain ε_{xx} ($x \parallel \mathbf{k}_{\mathrm{SAW}}$), transverse strain ε_{zz} (z perpendicular to the surface), and shear strain ε_{xz} (negligibly small close to the surface) [26]. In more sophisticated IDT architectures it is possible to excite overtone harmonics of the fundamental frequency, such as in the split-52 design [28], which is used in this work.

Optical time-resolved measurement of magnetization dynamics requires a fixed phase between the laser pulses and the acoustic bursts. The most common solution is a phase-locked loop [29]. The "master" clock imposes the repetition rate of the "slave" laser. The laser-cavity length is continuously adjusted to meet the set frequency. We propose a simpler, elegant, and low-cost alternative approach where f_{SAW} is built from the laser repetition rate, thereby ensuring a stable phase lock. Two research groups have very recently reported independently similar synchronization methods [18,27].

To generate the SAW rf, a small fraction of the output of a Ti:sapphire laser at a repetition rate (f_L) of approximately 75 MHz is directed to a silicon photodiode (Thorlabs PDA10A-EC, bandwidth 150 MHz) to pick up the laser fundamental frequency [Fig. 1(a)]. With the use of different rf multipliers, multiples of the laser frequency are then generated: nf_L, where $n = 2,\ 4,\ 6,\ 8$. To ensure that nf_L is free of any harmonics, the signal is filtered with 50-dB-rejection band-pass filters. The signal level is adjusted with a linear 40-dB amplifier and a set of attenuators.

The larger fraction of the 130-fs laser pulses (wavelength 722 nm) is sent to a pulse selector [Fig. 1(a)]. The repetition rate is reduced by a factor of 300 to $f_{\mathrm{rep}} = 250$ kHz. This beam is used to probe the magnetization and strain dynamics in a time window of 12 ns controlled with a motorized optical-delay-line stage.

As we see later, the IDT needs to be fed with a pulsed rf signal. To fabricate these pulses, the nf_L cw rf signal is mixed with a 400-ns-wide rectangular-pulse train from a pulse generator (Keysight 81150A) at the pulse-picker frequency f_{rep}, thus ensuring that both the envelope frequency and the rf of the SAW are commensurate with f_L. With the pulse generator we can modify the burst duration and its arrival time (electronic delay) at the transducer. The "edge-to-reference" jitter [30], defined as the timing variation between the rising edge of the rectangular pulse and the optical pulse, shows a standard deviation $\sigma = 13.1$ ps comfortably below 1% of the highest SAW period.

The linearly polarized laser pulses at f_{rep} are focused on the sample surface with a long-working-distance objective lens with numerical aperture of 0.4. The laser beam reflected off the sample travels through the same objective. The polarization rotation induced by the dynamical magnetization and strain components is detected by a balanced optical bridge relying on magneto-optical effects [17,31] and the photoelastic (PE) effect [26], respectively. The bridge output is demodulated by a lock-in amplifier at the frequency of a mechanical chopper ($f_{\mathrm{ch}} = 541$ Hz)

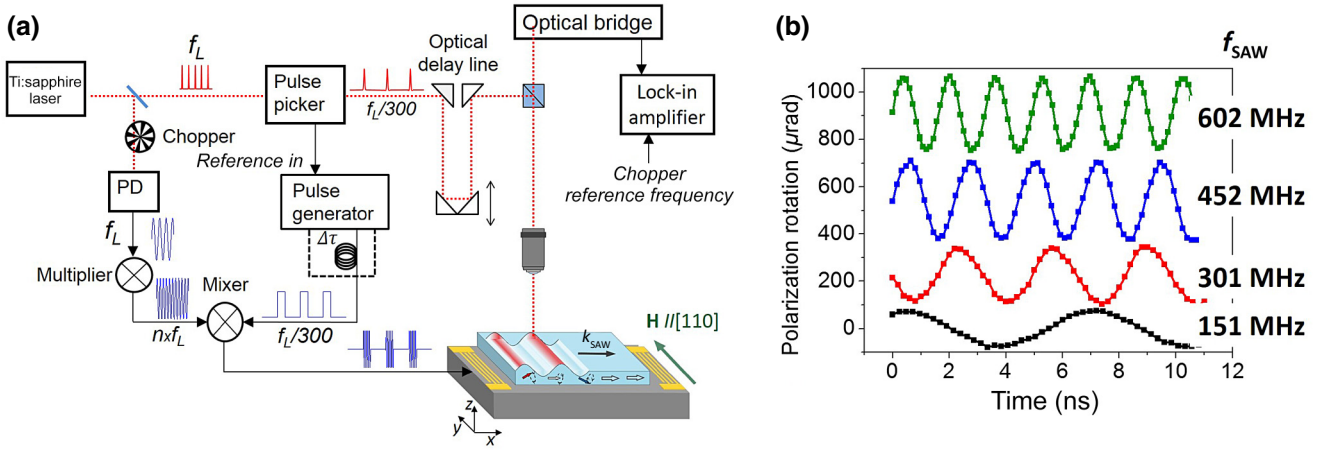

FIG. 1. (a) The experimental setup. (b) TRPR signal for four SAW frequencies (vertically offset for clarity). The probe polarization is set at 60° with respect to $\mathbf{k}_{\mathrm{SAW}}$, the applied magnetic field is 19.5 mT, and the temperature is 60 K. PD, photodiode.

inserted in the laser beam before the slow photodiode [Fig. 1(a)] (i.e., modulating the excitation rf). Polarization rotations as small as 0.1 μrad can be measured routinely.

The sample is a 45-nm-thick, in-plane-magnetized $Ga_{0.95}Mn_{0.05}As$ layer on a GaAs(001) substrate, annealed for 16 h at 200°C, with a Curie temperature of 120 K. It is placed in an Oxford Instruments MicroStat HiRes cryostat that ensures the required mechanical stability and optical access. The (Ga,Mn)As layer has a strong uniaxial magnetic anisotropy, with the easy axis along $[1\bar{1}0]$, and exhibits a large magnetoelastic coupling [16]. An in-plane magnetic field aligned with the hard axis [110] is applied to decrease the precession frequency and make it cross the SAW frequency. A 2×2 mm^2 mesa of (Ga,Mn)As is prepared by chemical etching. At two opposite ends a set of 42-nm-thick aluminum IDTs with 1-mm aperture are deposited on the GaAs [Fig. 1(a)]. To provide efficient operation of the IDTs even when the temperature is varied [given the temperature dependence of $v_R(T)$] and to achieve a compromise between excitation efficiency and bandwidth, the IDTs are designed as 25 pairs of split-52 electrodes. With a digit width and interdigit spacing of 1.9 μm, the fundamental period is $\lambda_{SAW} = 19$ μm. This ensures that the wavelength of all excited SAW frequencies is substantially greater than the laser-spot diameter (full width at half maximum of about 1 μm). The rf voltage applied to the IDT triggers the propagation of a SAW along the $[1\bar{1}0]$ axis. The rf power is set to 25 dBm for most of the data presented here. We use the second IDT to detect the SAW electrically by the inverse piezoelectric effect after it has traveled $d = 2.03$ mm along the layer surface. Figure 2 presents an oscilloscope trace of the recorded signal (red line). The first, 400-ns burst is the electromagnetic radiation. It travels with the speed of light and appears immediately at the receiver. After around $t_{trans} = d/v_R = 730$ ns the acoustic echo arrives ($v_R \approx 2780$ m s^{-1}). The pulsed rf allows the electromagnetic radiation and the acoustic echo to be separated in time. The rise time of the acoustic echo is defined by the IDT geometry, the SAW velocity, and the burst duration [26].

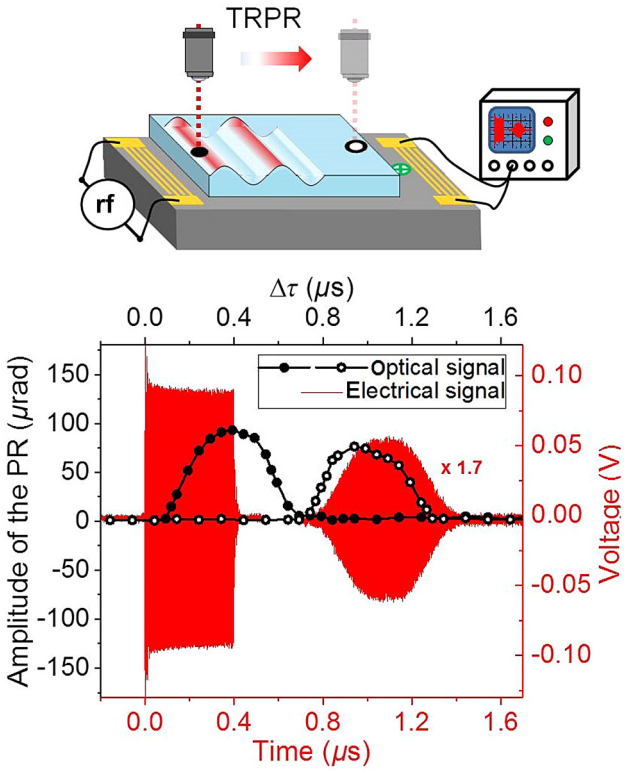

FIG. 2. Time-domain signal detected electrically (solid red line) by an oscilloscope, and amplitude of the optically detected TRPR oscillations (circles) as a function of the electronic delay. TRPR is measured in two places on the sample (open and solid circles in the scheme at the top). The crossed circle indicates where the optical SAW-induced-FMR data shown in Fig. 4(h) are taken. The surface amplitudes of the excited SAW strain components are $\varepsilon_{xx} = 4.8 \times 10^{-5}$ and $\varepsilon_{zz} = 2.2 \times 10^{-5}$, estimated following the procedure described in Ref. [16]. The SAW frequency is 452 MHz, the applied field $\mu_0 H$ is 20 mT, and the polarization angle β is 30°. PR, polarization rotation.

III. RESULTS AND DISCUSSION

Figure 1(b) shows the time-resolved polarization rotation (TRPR) at 60 K for SAW excitation frequencies of 151, 301, 452, and 602 MHz as a function of the optical delay. The frequency of the detected signals matches exactly the excitation frequency. The amplitude of the signal varies with the magnetic field up to the Curie temperature, above which we observe only a field-independent signal. This proves that the TRPR signal contains both a magnetic (field-dependent) contribution and a nonmagnetic one arising from the elasto-optical effect.

To prove that the optically detected dynamics is indeed triggered by the SAW, we monitor the amplitude of the TRPR signal at various delays after the beginning of the rf burst by setting an electronic delay $\Delta\tau$ between the electrical excitation and the optical pulse probe [Fig. 1(a)]. First the probe beam is set at 100 μm from the receiving IDT (1.9 mm from the emitter, open circle in the sample scheme in Fig. 2). The open-circle curve represents the amplitude of the TRPR oscillations versus the electronic delay. It has the same shape as the acoustic echo and peaks slightly before the arrival of this echo on the receiving IDT, in agreement with the location of the detection spot. Then the probe beam is positioned 67 μm from the emitter IDT (solid circle in the sample scheme in Fig. 2). The solid-circle curve represents the amplitude of the oscillations versus the electronic delay. It also has the same shape as the acoustic echo and is detected earlier, in agreement with the position of the detection spot. The 20% decrease in burst

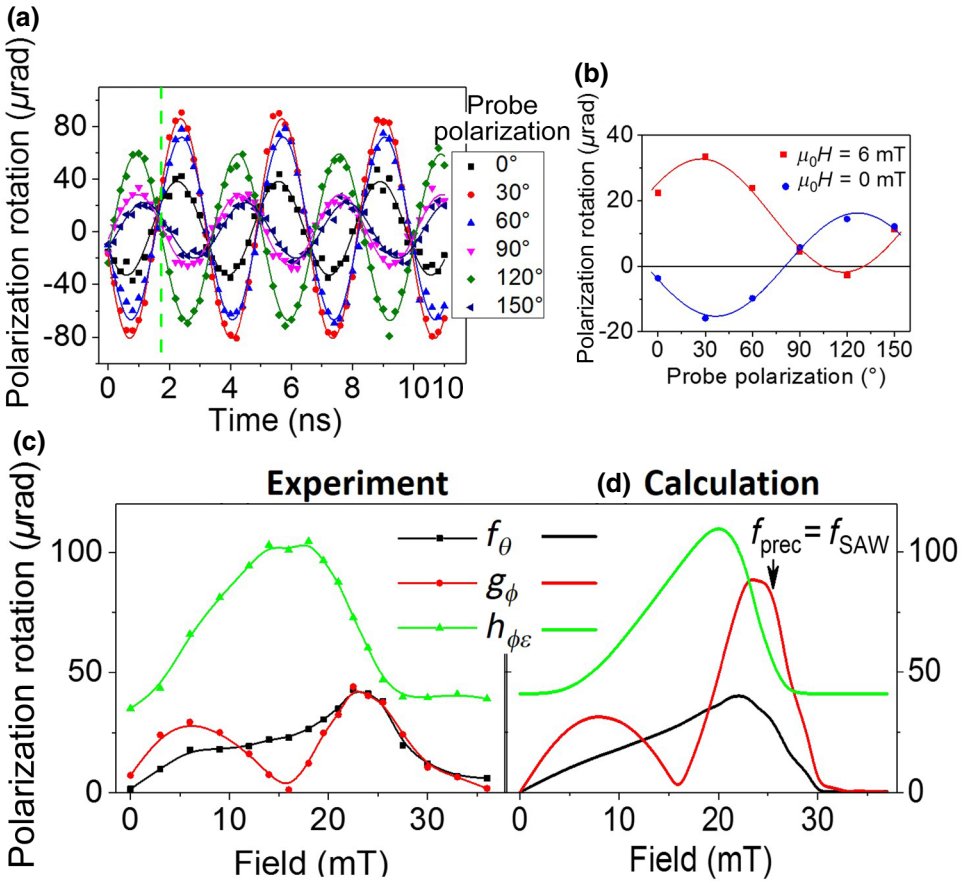

FIG. 3. Polarization and field dependence of the magnetization and strain dynamics for $f_{SAW} = 301$ MHz at $T = 60$ K. (a) TRPR signal for six polarization orientations as a function of the optical delay for $\mu_0 H = 6$ mT. (b) TRPR at fixed time delay [cross section of (a), dashed green line] versus probe polarization for two field values. (c) Field variation of the three components f_θ, g_ϕ, and $h_{\phi\varepsilon}$ related to the polar Kerr effect (β independent), MLD ($\cos 2\beta$ term), and mixed PE and MLD ($\sin 2\beta$ term), respectively, at $f_{SAW} = 301$ MHz. (d) Calculated amplitudes of f_θ, g_ϕ, and $h_{\phi\varepsilon}$; the parameters are $K = 18$ mrad, $V = 0.8$ mrad, and $P_E = 0.77$ rad, with $\varepsilon_{xx} = 5.3 \times 10^{-5}$. The Gaussian distribution of the in-plane anisotropy constant has a standard deviation equal to 12% of its mean value.

amplitude from one burst to the other can be directly correlated to the loss of acoustic amplitude via magnetoelastic interaction [see Fig. 4(g)]. For both spot positions, no signal is observed at the arrival time of the electromagnetic radiation. These results show that the TRPR signal is indeed generated by the SAW.

To disentangle the magneto-optical and elasto-optical contributions in the TRPR signal we analyze the dependence of the signal on the probe-light polarization and the applied magnetic field. The elasto-optical effect gives rise to a dynamic birefringence with axes parallel and perpendicular to the SAW wavevector $\mathbf{k}_{SAW}$. The resulting rotation of linear polarization is proportional to the P_{44} component of the elasto-optical tensor of the cubic GaAs and the ε_{xx} strain component [32–34]. It does not depend on the magnetic field. Besides, we expect a contribution from two magneto-optical effects [17,31]: the polar magneto-optical Kerr effect (PMOKE), which is sensitive to the out-of-plane dynamic component of the magnetization $\delta\theta$ and independent of the incoming polarization, and the (weaker) Voigt effect [magnetic linear dichroism (MLD)], which is sensitive to the in-plane dynamic component of the magnetization $\delta\phi$ and the field-dependent in-plane equilibrium orientation of the magnetization $\phi_0(H)$.

The TRPR signal can therefore be expressed as [17,26,31]

$$\begin{aligned}\delta\beta &= K\delta\theta(H,t) + 2V\delta\phi(H,t)\cos\{2[\beta-\phi_0(H)]\} \\ &\quad + P_E\varepsilon_{xx}(t)\sin 2\beta \\ &= K\delta\theta(H,t) + 2V\delta\phi(H,t)\cos 2\phi_0(H)\cos 2\beta \\ &\quad + [2V\delta\phi(H,t)\sin 2\phi_0(H) + P_E\varepsilon_{xx}(t)]\sin 2\beta, \end{aligned} \quad (1)$$

where β is the angle of the probe polarization with respect to $\mathbf{k}_{SAW}$, K and V are the Kerr and Voigt magneto-optical coefficients, respectively, and $P_E = \mathrm{Re}[n^3 P_{44}/(n^2-1)]$ is the elasto-optical coefficient, with n the refractive index. The experimental TRPR signal indeed shows a clear dependence on the probe polarization [Fig. 3(a)] and on the magnetic field [Fig. 3(b)]. For each time and field value, the signal is fitted as a function of β by $\delta\beta = F_\theta + G_\phi\cos 2\beta + H_{\phi\varepsilon}\sin 2\beta$. The resulting fit is very good, as seen in Fig. 3(b). The offset that appears under the application of a magnetic field $\mu_0 H = 6$ mT is related to the PMOKE signal $F_\theta = K\delta\theta$. The change of the phase is a good indication of the presence of MLD. The resulting F_θ, G_ϕ, and $H_{\phi\varepsilon}$ time-dependent functions are then fitted by sinusoidal functions with frequency f_{SAW}

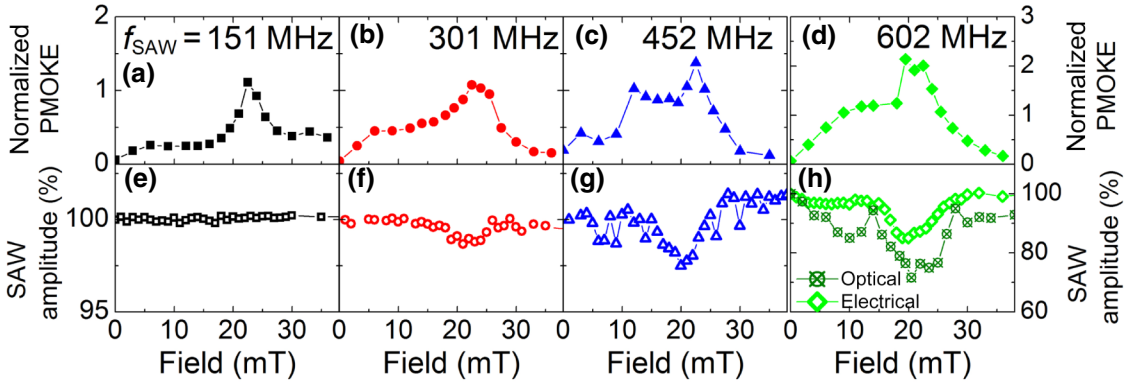

FIG. 4. (a)–(d) Field dependence of the PMOKE signal (out-of-plane magnetization dynamics) normalized by the field-independent PE signal for four SAW frequencies at $T = 60$ K. (e)–(h) Variation of the SAW amplitude with the magnetic field measured by acoustic-to-electrical conversion at the receiving IDT and in (h) normalized PE signal detected on GaAs in between the (Ga,Mn)As mesa and the receiving IDT [see the crossed circle in the scheme in Fig. 2], with polarization angle $\beta = 45^\circ$. The amplitudes of excited SAW strain components are estimated as $\varepsilon_{xx} = 5.3 \times 10^{-5}$ and $\varepsilon_{zz} = 1.8 \times 10^{-5}$ at $f_{SAW} = 301$ MHz (they are slightly different at other frequencies but are low enough to stay in the linear regime).

to extract the field dependence of their amplitudes f_θ, g_ϕ, and $h_{\phi\varepsilon}$, respectively. We have $f_\theta = K\delta\theta_0(H)$ and $g_\phi = 2V\delta\phi_0(H)|\cos 2\phi_0(H)|$, where $\delta\theta_0$ and $\delta\phi_0$ are the amplitudes of the oscillating $\delta\theta(t)$ and $\delta\phi(t)$, respectively.

In Fig. 3(c) we plot the amplitudes f_θ, g_ϕ, and $h_{\phi\varepsilon}$ as a function of the applied field. The amplitude of the PMOKE signal f_θ (black curve) increases progressively to reach a maximum at 22.5 mT and then drops to zero. The MLD component g_ϕ (red curve) shows a different behavior, with two maxima and a zero at $\mu_0 H = 16$ mT. The $h_{\phi\varepsilon}$ component, reflecting a combination of PE and MLD (green curve), has a broad maximum and a clear 40-μrad offset owing to the field-independent elasto-optical effect.

To demonstrate that the physics of the magnetoelastic coupling is responsible for the experimental observations, the magnetization dynamics is modeled in the framework of the Landau-Lifshitz-Gilbert equation including the driving torque generated by the SAW [20]. When the SAW is traveling along $[1\bar{1}0]$, the torque is driven mainly by the ε_{xx} strain component [16]. We use the sample magnetic parameters (magnetization and magnetic anisotropy) obtained from vibrating-sample-magnetometer and cavity-FMR experiments. The calculated amplitudes [35] of the magneto-optical signals f_θ and g_ϕ [Fig. 3(d), black and red curves, respectively] show a peak around 25 mT, corresponding to the resonance condition of equal precession and SAW frequencies at $f_{SAW} = 301$ MHz. The g_ϕ amplitude (red curve) goes to zero at a field such that the static magnetization is at 45° to the easy axis ($\cos 2\phi_0 = 0$). The baseline for $h_{\phi\varepsilon}$ is given by the PE effect, which does not depend on the magnetic field. As seen from the comparison of Figs. 3(c) and 3(d), good quantitative agreement between experimental and calculated f_θ, g_ϕ, and $h_{\phi\varepsilon}$ curves is obtained. To account for the amplitude and width of f_θ, g_ϕ, and $h_{\phi\varepsilon}$ we have to introduce a dispersion of the uniaxial in-plane magnetic anisotropy constant, which is known to be crucial for SAW-induced magnetization dynamics [16]. These results show that we are able to disentangle the different contributions in the optical polarization signal and to accurately extract the dynamical magnetic contribution. They provide direct, time-domain detection of magnetoacoustic resonance induced by electrically generated *propagating* SAWs. The resonant coupling of optically generated *stationary* SAWs with magnetization was previously evidenced by Faraday effect in nickel [5,10,13]. In our system, the presence of Kerr and Voigt effects, moreover, gives access to the in-plane and the out-of-plane components of the magnetization dynamics.

To compare the sensitivity of the magneto-optical signal detection and the SAW-amplitude detection after propagation along the layer, we show in Fig. 4 the PMOKE component f_θ (out-of-plane magnetization dynamics) and the variation of the electrically detected SAW amplitude (through the receiving IDT) as a function of the applied magnetic field for the four SAW frequencies. The PMOKE data [Figs. 4(a)–4(d)] are normalized by the measured PE level (field-independent baseline of $h_{\phi\varepsilon}$) to correct for slightly different SAW amplitudes. For each frequency we observe a clear and strong peak of the PMOKE curve at the resonance field (which has similar values for the four frequencies because of the steep variation of the FMR frequency with the field [16]). The electrically detected SAW amplitude [Figs. 4(e)–4(h)] is a rather noisy signal at 151, 301, and 452 MHz, with a much smaller dynamical range. At $f_{SAW} = 301$, 452, and 602 MHz, it shows a dip at the same field as the peak of the corresponding PMOKE signal. The dip is more pronounced at the highest frequency of 602 MHz as expected from the increase of

the absorbed SAW power with the SAW frequency [1,16]. The dip is, however, not detectable at $f_{SAW} = 151$ MHz, whereas the PMOKE peak is clearly detected. We also plot in Fig. 4(h) the amplitude of the PE signal detected on GaAs, in between the (Ga,Mn)As mesa and the receiving IDT (crossed circle in the scheme in Fig. 2), normalized by its low-field value. The data are taken for an incoming beam polarization of 45°, which maximizes the strain-induced birefringence. Its field dependence is similar to that of the electrical signal [Fig. 4(h)] in shape and amplitude. These results show the much larger dynamical range and sensitivity of the magneto-optical SAW-induced FMR signal, because it is detected on a zero background, with respect to the electrical or optical signal of the SAW amplitude variation, which is detected on a nonzero background.

IV. CONCLUSION

We have developed a sensitive time-domain optical technique to investigate the magnetoelastic coupling between piezoelectrically generated traveling SAWs and magnetization in ferromagnetic layers at variable temperature. The time-resolved magnetization precession is clearly proved to originate from the magnetoelastic coupling with the SAW and shows a resonant behavior at equal SAW and precession frequencies. Compared with the detection of the SAW attenuation, the magneto-optical time-resolved SAW-induced FMR signal is more sensitive and provides a greater signal-to-noise ratio. The detection threshold of the time-resolved signal is mainly governed by the convolution of the SAW wavelength and the laser-spot size w. As such, magnetization precession can still be observed at $f_{SAW} = 900$ MHz, for which $\lambda_{SAW} \sim 3w$. Working at higher SAW frequencies (above 1 GHz) will require a tighter focusing of the laser spot, by working at higher photon energy (keeping a decent Kerr signal) and/or by increasing the numerical aperture of the focusing objective (keeping a good linear polarization). More generally, we believe that this approach, combining high space and time sensitivity and access to the two components of magnetization, will find wider use in any experiment requiring the synchronization of a rf electrical stimulus with the ultrafast optical detection of the magnetic effects it induces, and should benefit broadly the magnetization dynamics community. Applied to magnetostrictive materials, this technique opens the way for a deeper insight into the magnon-phonon coupling and the exploration of the nonlinear regime of acoustic-wave-induced magnetization dynamics. Since electrically generated SAWs are a well-mastered technology in microelectronics, SAW-induced magnetization control could be readily implemented in logic or memory devices, with the unprecedented possibility to use wave-physics tools such as focusing, diffraction, and wave guiding to address a magnetic bit.

ACKNOWLEDGMENTS

This work was supported by the Agence Nationale de la Recherche (Grant No. ANR13-JS04-0001-01). The authors also acknowledge D. Hrabovsky (MPBT - Mesures Physiques à Basses Températures-Physical Properties Low-Temperature Facility of Sorbonne University) for help with the magnetometry experiments, H.J. von Bardeleben (Institut des Nanosciences de Paris) for cavity FMR measurements, and C. Testelin (Institut des Nanosciences de Paris) for providing scientific equipment.

[1] L. Dreher, M. Weiler, M. Pernpeintner, H. Huebl, R. Gross, M. S. Brandt, and S. T. B. Goennenwein, Surface acoustic wave driven ferromagnetic resonance in nickel thin films: Theory and experiment, Phys. Rev. B **86**, 134415 (2012).

[2] M. Bombeck, A. Salasyuk, B. Glavin, A. V. Scherbakov, C. Brüggemann, D. R. Yakovlev, V. Sapega, X. Liu, Jacek K. Furdyna, A. V. Akimov, and M. Bayer, Excitation of spin waves in ferromagnetic (Ga,Mn)As layers by picosecond strain pulses, Phys. Rev. B **85**, 195324 (2012).

[3] W. Li, B. Buford, A. Jander, and P. Dhagat, Acoustically assisted magnetic recording: A new paradigm in magnetic data storage, IEEE Trans. Mag. **50**, 37 (2014).

[4] L. Thevenard, C. Gourdon, J.-Y. Prieur, H. J. von Bardeleben, S. Vincent, L. Becerra, L. Largeau, and J.-Y. Duquesne, Surface acoustic wave-driven ferromagnetic resonance in (Ga,Mn)(As,P) epilayers, Phys. Rev. B **90**, 094401 (2014).

[5] Y. Yahagi, B. Harteneck, S. Cabrini, and H. Schmidt, Controlling nanomagnet magnetization dynamics via magnetoelastic coupling, Phys. Rev. B **90**, 140405 (2014).

[6] K. Shen and G. E. Bauer, Laser-Induced Spatiotemporal Dynamics of Magnetic Films, Phys. Rev. Lett. **115**, 197201 (2015).

[7] S. Davis, J. A. Borchers, B. B. Maranville, and S. Adenwalla, Fast strain wave induced magnetization changes in long cobalt bars: Domain motion versus coherent rotation, J. Appl. Phys. **117**, 063904 (2015).

[8] P. G. Gowtham, T. Moriyama, D. C. Ralph, and R. A. Buhrman, Traveling surface spin-wave resonance spectroscopy using surface acoustic waves, J. Appl. Phys. **118**, 233910 (2015).

[9] P. Chowdhury, P. Dhagat, and A. Jander, Parametric amplification of spin waves using acoustic waves, IEEE Trans. Mag. **51**, 1300904 (2015).

[10] J. Janušonis, C. L. Chang, P. H. M. van Loosdrecht, and R. I. Tobey, Frequency tunable surface magneto-elastic waves, Appl. Phys. Lett. **106**, 181601 (2015).

[11] L. Thevenard, I. S. Camara, J.-Y. Prieur, P. Rovillain, A. Lemaıtre, C. Gourdon, and J.-Y. Duquesne, Strong reduction of the coercivity by a surface acoustic wave in an out-of-plane magnetized epilayer, Phys. Rev. B **93**, 140405 (2016).

[12] L. Thevenard, I. S. Camara, S. Majrab, M. Bernard, P. Rovillain, A. Lemaître, C. Gourdon, and J.-Y. Duquesne, Precessional magnetization switching by a surface acoustic wave, Phys. Rev. B **93**, 134430 (2016).

[13] C. L. Chang, A. M. Lomonosov, J. Janusonis, V. S. Vlasov, V. V. Temnov, and R. I. Tobey, Parametric frequency mixing in a magnetoelastically driven linear ferromagnetic resonance oscillator, Phys. Rev. B **95**, 060409 (2017).

[14] Y. Hashimoto, S. Daimon, R. Iguchi, Y. Oikawa, K. Sato, D Bossini, K. Shen, Y. Tabuchi, T. Satoh, B. Hillebrands, G. E. W. Bauer, T. H. Johansen, A. Kirilyuk, T. Rasing, and E. Saitoh, All-optical observation and reconstruction of spin wave dispersion, Nat. Commun. **8**, 15859 (2017).

[15] J.-W. Kim and J.-Y. Bigot, Magnetization precession induced by picosecond acoustic pulses in a freestanding film acting as an acoustic cavity, Phys. Rev. B **95**, 144422 (2017).

[16] P. Kuszewski, I. S Camara, N. Biarrotte, L. Becerra, J. von Bardeleben, W. Savero Torres, A. Lemaître, C. Gourdon, J.-Y. Duquesne, and L. Thevenard, Resonant magneto-acoustic switching: influence of Rayleigh wave frequency and wavevector, J. Phys.: Cond. Mat. **30**, 244003 (2018).

[17] S. Shihab, L. Thevenard, A. Lemaître, and C. Gourdon, Counter-rotating standing spin waves: A magneto-optical illusion, Phys. Rev. B **95**, 144411 (2017).

[18] M. Foerster *et al.*, Direct imaging of delayed magneto-dynamic modes induced by surface acoustic waves, Nat. Comm. **8**, 407 (2017).

[19] T. L. Linnik, A. V. Scherbakov, D. R. Yakovlev, X. Liu, J. K. Furdyna, and M. Bayer, Theory of magnetization precession induced by a picosecond strain pulse in ferromagnetic semiconductor (Ga,Mn)As, Phys. Rev. B **84**, 214432 (2011).

[20] L. Thevenard, J.-Y. Duquesne, E. Peronne, H. J. von Bardeleben, H. Jaffres, S. Ruttala, J.-M. George, A. Lemaître, and C. Gourdon, Irreversible magnetization switching using surface acoustic waves, Phys. Rev. B **87**, 144402 (2013).

[21] L. Y. Yeo and J. R. Friend, Surface acoustic wave microfluidics, Annu. Rev. Fluid Mech. **46**, 379 (2014).

[22] A. V. Mamishev, K. Sundara-Rajan, F. Yang, Y. Du, and M. Zahn, Interdigital sensors and transducers, Proc. IEEE **92**, 808 (2004).

[23] T. Poole and G. R. Nash, Acoustoelectric current in graphene nanoribbons, Sci. Rep. **7**, 1767 (2017).

[24] M. M. De Lima and P. V. Santos, Modulation of photonic structures by surface acoustic waves, Rep. Prog. Phys. **68**, 1639 (2005).

[25] A. Neubrand and P. Hess, Laser generation and detection of surface acoustic waves: Elastic properties of surface layers, J. Appl. Phys. **71**, 227 (1992).

[26] D. Royer and E Dieulesaint, *Elastic Waves in Solids II. Generation, Acousto-optic Interaction, Application* (Springer-Verlag, Berlin, 2000).

[27] M. Weiß, A. L. Hörner, E. Zallo, P. Atkinson, A. Rastelli, O. G. Schmidt, A. Wixforth, and H. J. Krenner, Multiharmonic frequency-chirped transducers for surface-acoustic-wave optomechanics, Phys. Rev. Appl. **9**, 014004 (2018).

[28] F. J. R. Schülein, E. Zallo, P. Atkinson, O. G. Schmidt, R. Trotta, A. Rastelli, A. Wixforth, and H. J. Krenner, Fourier synthesis of radiofrequency nanomechanical pulses with different shapes, Nat. Nanotechnol. **10**, 512 (2015).

[29] R. B. Holländer, C. Müller, M. Lohmann, B. Mozooni, and J. McCord, Component selection in time-resolved magneto-optical wide-field imaging for the investigation of magnetic microstructures, J. Magn. Magn. Mater. **432**, 283 (2017).

[30] W. Maichen, *Digital Timing Measurements: From Scopes and Probes to Timing and Jitter* (Springer Science & Business Media, 2006).

[31] P. Němec, F. Trojanek, E. Rozkotova, N. Tesarova, E. De Ranieri, K. Olejnik, J. Zemen, V. Novak, M. Cukr, P. Maly, and T. Jungwirth, Experimental observation of the optical spin transfer torque, Nat. Phys. **8**, 411 (2012).

[32] D. Royer and E. Dieulesaint, *Elastic Waves in Solid I: Free and Guided Propagation* (Springer-Verlag, Berlin Heidelberg, 2000).

[33] T. Saito, O. Matsuda, M. Tomoda, and O. B. Wright, Imaging gigahertz surface acoustic waves through the photoelastic effect, J. Opt. Soc. Am. B **27**, 2632 (2010).

[34] P. V. Santos, Acoustic field mapping on GaAs using microscopic reflectance and reflectance anisotropy, Appl. Phys. Lett. **74**, 4002 (1999).

[35] Because we are only considering the uniform FMR mode, it is unecessary to take into account the absorption and optical phase shift of the light in the layer, as in Ref. [17].